DTIC FILE COPY

(2)

SECURITY CLASSIFIC

AD-A200 202

...N PAGE

Form Approved
OMB No. 0704-0188

1a. REPORT SECURI: Unclassif

1b. RESTRICTIVE MARKINGS

2a. SECURITY CLAS:

AUG 25 1988

3. DISTRIBUTION/AVAILABILITY OF REPORT
Approved for public release; distribution unlimited

2b. DECLASSIFICATION/DOWNGRADING SCHEDULE

4. PERFORMING ORGANIZATION REPORT NUMBER(S)
UMSC - 88-C-AF 2

5. MONITORING ORGANIZATION REPORT NUMBER(S)
AFOSR-TR- 88-0918

6a. NAME OF PERFORMING ORGANIZATION
University of Michigan, Ann Arbor

6b. OFFICE SYMBOL (If applicable)

7a. NAME OF MONITORING ORGANIZATION
AFOSR/NE

6c. ADDRESS (City, State, and ZIP Code)
Ann Arbor, MI 48109

7b. ADDRESS (City, State, and ZIP Code)
Bldg 410
Bolling AFB, DC 20332

8a. NAME OF FUNDING/SPONSORING ORGANIZATION
Air Force Office of Scientific Research

8b. OFFICE SYMBOL (If applicable)

9. PROCUREMENT INSTRUMENT IDENTIFICATION NUMBER
Grant No. AFOSR-87-0289

8c. ADDRESS (City, State, and ZIP Code)
AFOSR/NE, Bldg. 410, Bolling AFB, DC20332-6448 Dr. Rosenstein

10. SOURCE OF FUNDING NUMBERS

PROGRAM ELEMENT NO.	PROJECT NO.	TASK NO	WORK UNIT ACCESSION NO.
61102F	2306	A2	

11. TITLE (Include Security Classification)
Mechanistic Studies of Pressure-Assisted Superplasticity of Structural Ceramics

12. PERSONAL AUTHOR(S)
Chen, I-Wei

13a. TYPE OF REPORT	13b. TIME COVERED	14. DATE OF REPORT (Year, Month, Day)	15. PAGE COUNT
Annual Tech./Scientific Report	FROM 6/15/87 TO 6/14/88	7/15/88	28

16. SUPPLEMENTARY NOTATION

17. COSATI CODES			18. SUBJECT TERMS (Continue on reverse if necessary and identify by block number)
FIELD	GROUP	SUB-GROUP	

19. ABSTRACT (Continue on reverse if necessary and identify by block number)

Superplastic flow in silicon nitride ceramics containing YAG was investigated. A low flow stress was found possible when the solid SIALON grains are included in the liquid phase YAG above a critical temperature. The mechanisms of grain growth and microstructural development in silicon nitride and zirconia were studied. The effect of (Mn) addition on lowering the forming temperature of zirconia was demonstrated.

(Mn) Manganese

20. DISTRIBUTION/AVAILABILITY OF ABSTRACT
☒ UNCLASSIFIED/UNLIMITED ☐ SAME AS RPT ☐ DTIC USERS

21. ABSTRACT SECURITY CLASSIFICATION
Unclassified

22a. NAME OF RESPONSIBLE INDIVIDUAL
Scholes

22b. TELEPHONE (Include Area Code)
(202)767-4933

22c. OFFICE SYMBOL
NE

DD Form 1473, JUN 86 — Previous editions are obsolete. — SECURITY CLASSIFICATION OF THIS PAGE

88 8 25 061

I. Objectives

The goal of this program is to identify the key elements that facilitate superplastic forming of structural ceramics, and to characterize and control the damage and microstructure evolution during forming and post-forming heat treatment. Single and multi-phase (including a liquid phase) microstructures will be obtained and investigated in the candidate ceramics of silicon nitride, zirconia monolithic and zirconia composites for the above purpose. During the first year of this program, we have demonstrated the presence of superplastic flow in a series of YAG-containing β SIALON, identified the grain growth mechanisms in both SIALON and zirconia, and discovered a pronounced effect of Mn doping in lowering the sintering, and hence forming, temperature of Y-stabilized zirconia.

2. SIALON Ceramics

Solid solutions of Si_3N_4 with Al_2O_3:AlN form a series of β SIALON of a composition $Si_{6-x}Al_{8-x}N_{8-x}O_x$, with Al substituting Si and O substituting N in the β Si_3N_4 structure. A garnet phase, $Y_3Al_5O_{12}$ (YAG), can be added to the SI, Al, N, O system to form a liquid phase at the sintering temperature which can then be fully crystallized along the grain boundary by post-sinter annealing. Although the equilibrated β SIALON grains are large and elongated, and thus not amenable to superplastic forming, they are initially small and equiaxed during liquid phase sintering. We found that the most favorable microstructure could be produced by sintering, at relatively low temperatures, a slip-cast green-body formed by pressure-filtration. Two SIALON phases were present after sintering forming a duplex microstructure. A series of such ceramics, containing different amounts of garnet phase, were prepared and used for the scoping experiment to demonstrate superplasticity.

Two modes of deformation akin to superplasticity were identified. The first mode, which operates at lower temperatures, can be attributed to the diffusional creep of fine SIALON grains which is aided by the grain boundary liquid YAG phase. A typical stress vs strain rate plot, as shown

in Fig. 1, features a flat low strain rate regime controlled by a threshold stress, and an intermediate strain rate regime of a strain rate sensitivity m=0.67. Such high strain rate sensitivity is characteristic of a diffusion controlled superplastic flow. At the 1400°C test temperature, the amount of the liquid phase is probably negligible. The temperature dependence of the flow stress is shown in Fig. 2.

The second mode, which operates at higher temperatures, can be attributed to the viscous flow of the liquid YAG phase which contains a large amount of isolated solid SIALON grains. A prerequisite of this deformation mode is the breaking up of the solid SIALON polycrystal network which can be accomplished by applying a sufficiently large shear stress. As shown in Fig. 3, in a SIALON which contains up 10 v/o YAG at 1450°C, the flow stress initially increases with the strain rate, reaching 300MPa before an abrupt drop to 50 MPa. Apparently, at the upper flow stress, the solid network breaks up and each individual grain is then surrounded by a liquid phase which flows at a much lower stress. This process can also be accomplished by increasing the test temperature. As shown in Fig. 4, in a SIALON which contains 20 v/o YAG, an increase of 25°C causes a decrease of flow stress by more than an order of magnitude, to merely 30 MPa even at very high strain rates. The temperature where softening of SIALON-YAG occurs is dependent on the YAG content, as shown in Fig. 5. At, or slightly above, the softening temperature, the second mode of deformation controlled by viscous flow of YAG can easily take place. (Overheating may result in a total melt-down and is not desirable.)

We suggest that these scoping experiments demonstrate the potential of superplastic forming of silicon nitride ceramics. Clearly, control of the phase relation and microstructure is important in order to take full advantage of the lower flow stress of the liquid phase. In view of the relatively low processing temperature and flow stress achieved in the present experiments, we are optimistic that further optimization of the microstructure and composition would yield even more favorable forming conditions. This aspect will be pursued in future work along with a more thorough characterization of the constitutive flow relations.

To understand the processing conditions necessary to obtain the most desirable initial microstructures, and to ascertain the stability of fine grains against coarsening at hot forming temperatures, we have undertaken a systematic study of grain growth kinetics and sintering aids for SIALON and zirconia. As detailed in Appendix 1, kinetics of the anisotropic grain growth of β SIALON were determined and found to follow a cubic growth law. A high resolution TEM examination revealed a rounded growth front along the [001] direction and a sharp interface with very few ledges along the [210] direction. A growth model, which envisions continuous growth in the [001] direction and lateral ledge growth in the [210] direction, appears to provide a satisfactory explanation of these observations.

It has also been recently reported in Japanese literature that overpressure sintering of SIALON produced grains of very high aspect ratios seemed to offer superior fracture toughness. It is not clear whether the effect is kinetic, due to the higher sintering temperature afforded by the overpressure, or thermodynamic due to the added nitrogen driving force afforded by the overpressure. We have initiated an experiment, using the overpressure nitrogen furnace at the Army Materials Technology Laboratory in Watertown, MA, to try to resolve the above issue.

3. Zirconia Ceramics

ZrO_2 forms solid solutions with a large number of oxides containing cations of either a larger radius or a lower valence, resulting in a series of partially or fully stabilized alloys. If only the tetragonal phase is present, the alloy is known as a tetragonal zirconia polycrystal (TZP). At a higher stabilizer content, the high temperature polymorph, cubic phase, is also present. The first superplastic crystalline ceramic was reported in an (3 m/o) yttria stabilized zirconia containing mainly tetragonal grains and a small amount (c.a. 10%) of cubic grains. Apparently, it is the relatively small and stable grain size, of the order of 0.3 micron, which can be routinely obtained in such alloy that makes the material superplastic, as has been confirmed by many groups in the last two years.

While TZP usually has fine grains, the cubic grains are normally much larger. This peculiar behavior has been noticed by a large number of ceramists, but gone unexplained. To control and facilitate the microstructural development favorable for superplastic forming of zirconia ceramics, it is necessary to understand the above phenomenon in more detail. In Appendix 2, the kinetics of sintering and grain growth in tetragonal and cubic zirconia are reported and found to follow a parabolic growth law. Growth rates of cubic grains are shown to be 30 to 250 times faster than that of tetragonal grains, while the activation energy is higher in tetragonal zirconia. Measurements of dihedral angles also revealed a larger grain boundary energy in the cubic phase than in the tetragonal phase.

To explore the generality of the behavior described above, we have further examined other zirconia systems stabilized by In_2O_3 and Sc_2O_3, which have different cation radii but the same charge. The intent here is to examine any possible role of strain energies of misfitting ions or phases. It was found that in all cases, the cubic phase grew much faster than the tetragonal phase. Moreover, through dihedral angle measurements, as summarized in Table 1, we found the same ratio of interfacial energies among different phases to hold for all the systems studied. It thus seems that there is a common cause for the different grain growth behavior of cubic and tetragonal zirconia, independent of their ionic radii of solutes.

The possible connection between the above behavior and solute segregation is currently being explored. Spatial distribution of solutes of various ionic radii and charges in both phases are being examined. Initial efforts using ESCA have produced encouraging results showing a clear segregation characteristic to grain boundaries, and that the level of segregation is sensitive to the phases and charges of the segregants. More results are being collected at the present time in order to provide a data base to construct a realistic model.

Related to sintering and grain growth in zirconia is the discovery that Mn doping can substantially lower the sintering temperature, to c.a. 1200°C, for both cubic and tetragonal zirconia. This is shown in Fig. 6. A slight

advantage of a reducing atomsphere, which aids sintering in this case, was also observed, as illustrated by the dilatometry curves in Fig. 7. The latter effect is probably due to a change of the oxidation state of Mn. A detailed determination of sintering and growth kinetics, as shown in Figs. 8-10, found an essentially parabolic grain growth in Mn-doped tetragonal zirconia at all temperatures, with an activation energy close to that of the undoped material given in Appendix 2. In cubic zirconia, the parabolic growth law broke down above 1500°C, possibly due to the formation of a liquid phase.

These finding prompted us to prepare dense zirconia ceramics at below 1250°C, with a very fine grain size. Since our past experience suggests that a lower sintering temperature generally presages a lower superplastically forming temperature, we are hopeful that such zirconia, with appropriate doping, could be superplastically deformed at or below 1200°C, i.e. at least 200°C lower than those previously reported in literature. Such developments should prove technologically significant and are currently being pursued in the program.

4. List of Publications and Presentations

1. "Anisotropic Grain Growth During Final State Sintering of Silicon Nitride Ceramics", C.M. Hwang, T.Y. Tien, and I-Wei Chen, to be published in Sintering 1987, ed. S. Somiya, Elsevier Pub. Co.

2. "Sintering and Grain Growth in Tetragonal and Cubic Zirconia", I.G. Lee and I-Wei Chen, to be published in Sintering 1987, ed. S. Somiya, Elsevier Pub. Co.

3. "Grain Growth in Tetragonal and Cubic Zirconia", presented by I.G. Lee at the 90th Annual Meeting of The American Ceramic Society, Cincinnati, OH., May, 1988.

4. "Superplastic Forming of Structural Ceramics", invited talk to be presented by I-Wei Chen at the U.S. Japan Joint Workshop on Ceramic Processing, Seattle, WA., August, 1988.

Table 1. Dihedral angles and interfacial energies of zirconia

Stabilizer	Y_2O_3 4m/o	Y_2O_3 6m/o	Y_2O_3+Mn_3O_4 6m/o	In_2O_3 5.5m/o	Sc_2O_3 5m/o
θ_{tt}	134°±7°	131±7°	134±6°	136±6°	140±8°
θ_{cc}	97±11°	105±10°	107±19°	95±9°	113±14°
γ_{cc}/γ_{tt}	1.7	1.5	1.5	1.8	1.6
γ_{ct}/γ_{tt}	1.3	1.2	1.3	1.3	1.5

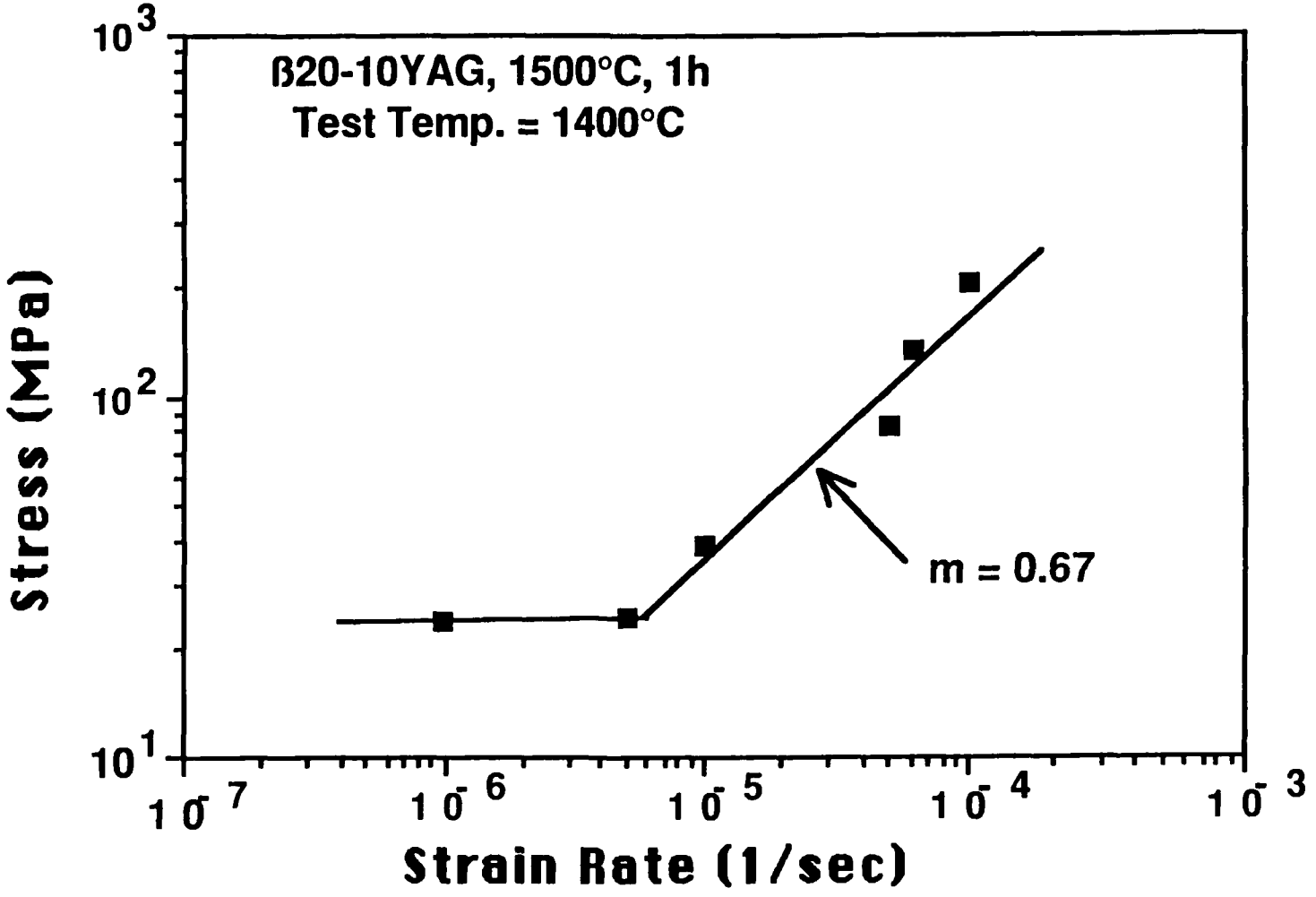

Fig. 1 Stress vs strain rate in ß 20 - 10 YAG at 1400°C

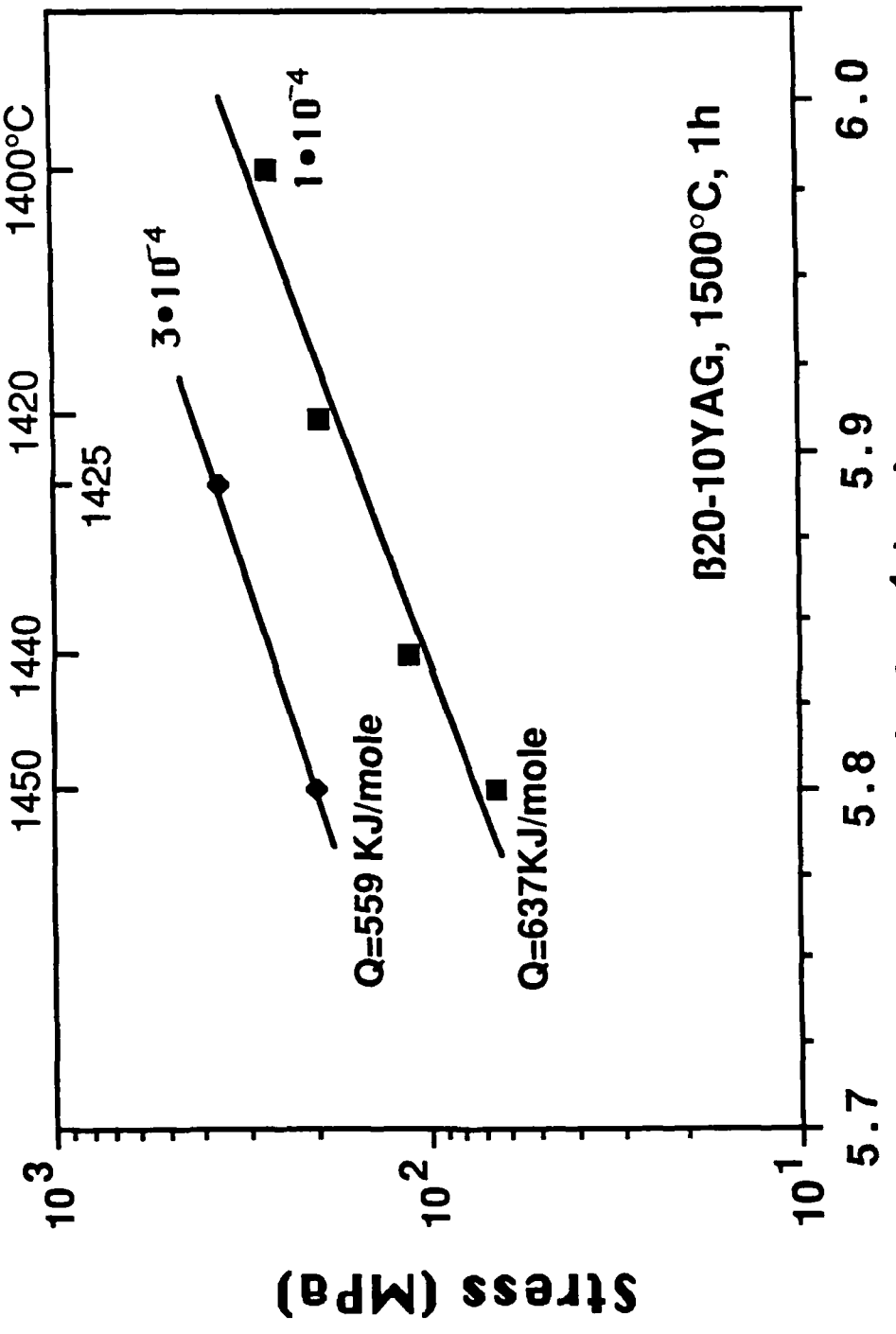

Fig. 2 Temperature dependence of flow stress of ß 20 - 10 YAG

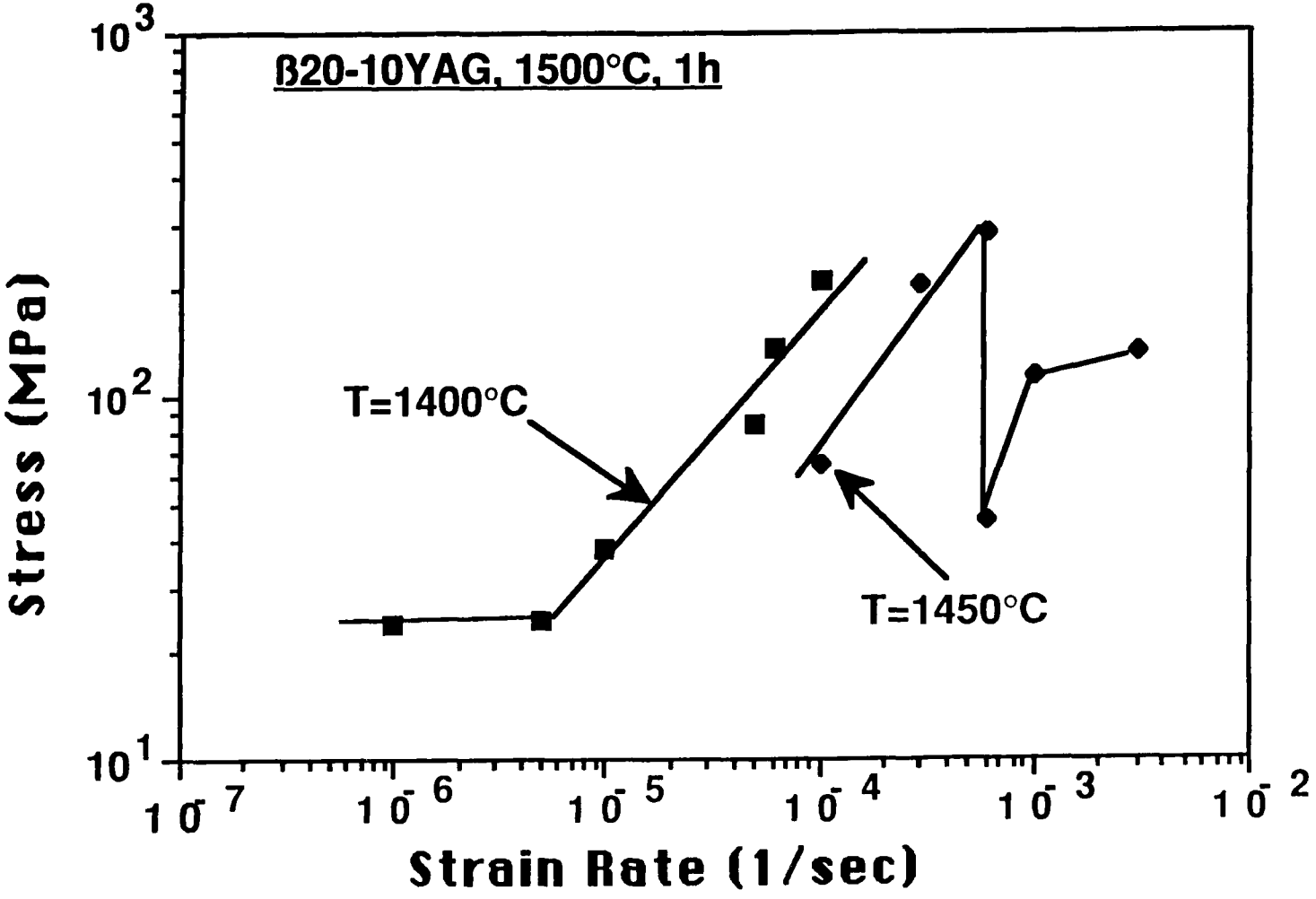

Fig. 3 Stress vs strain rate of ß 20 - 10 YAG at 1400°C and 1450°C
(Note the transition at strain rate 5×10^{-4}/sec.)

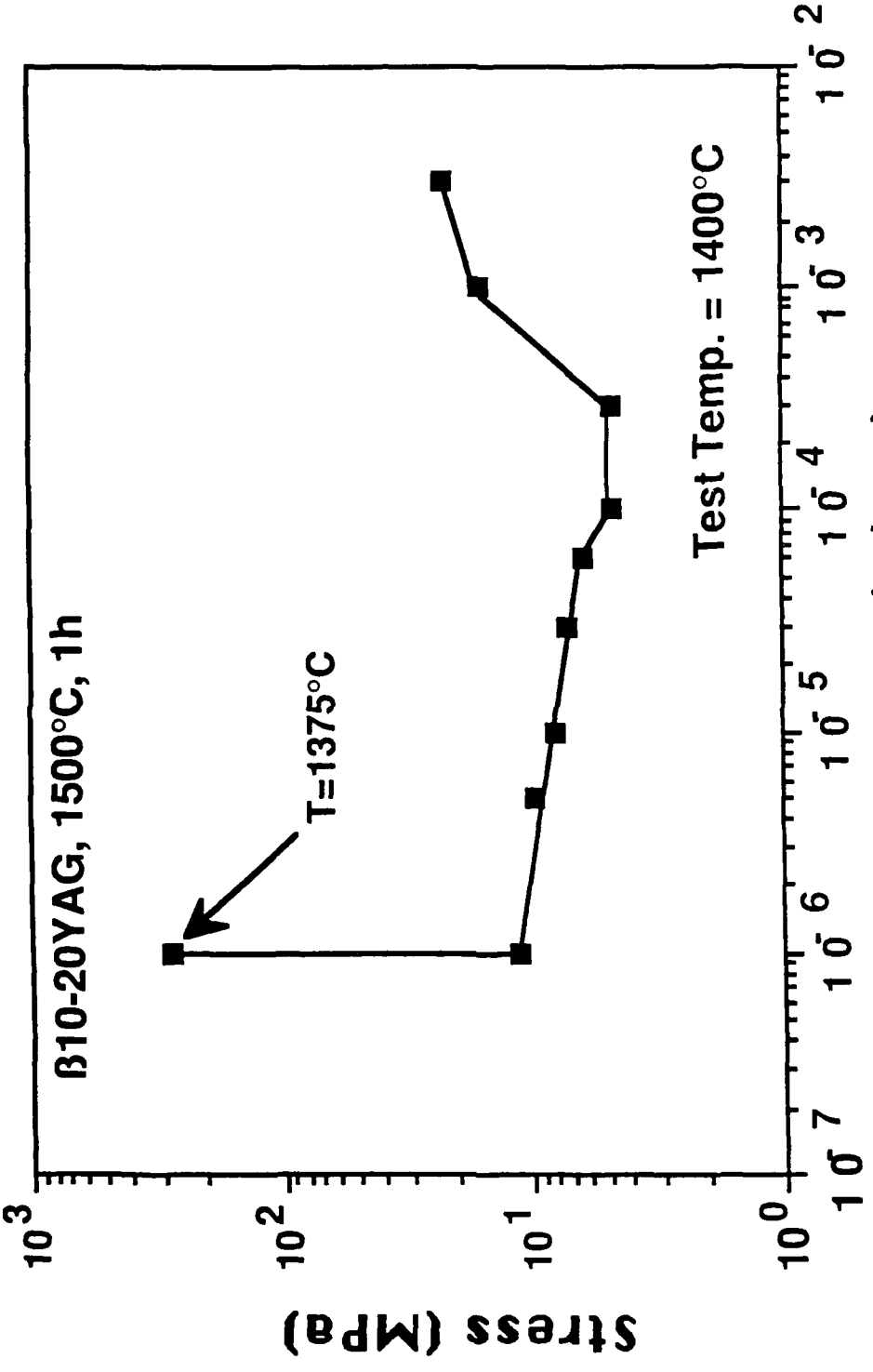

Fig. 4 Stress vs strain rate in ß 10 - 20 YAG at 1400°C

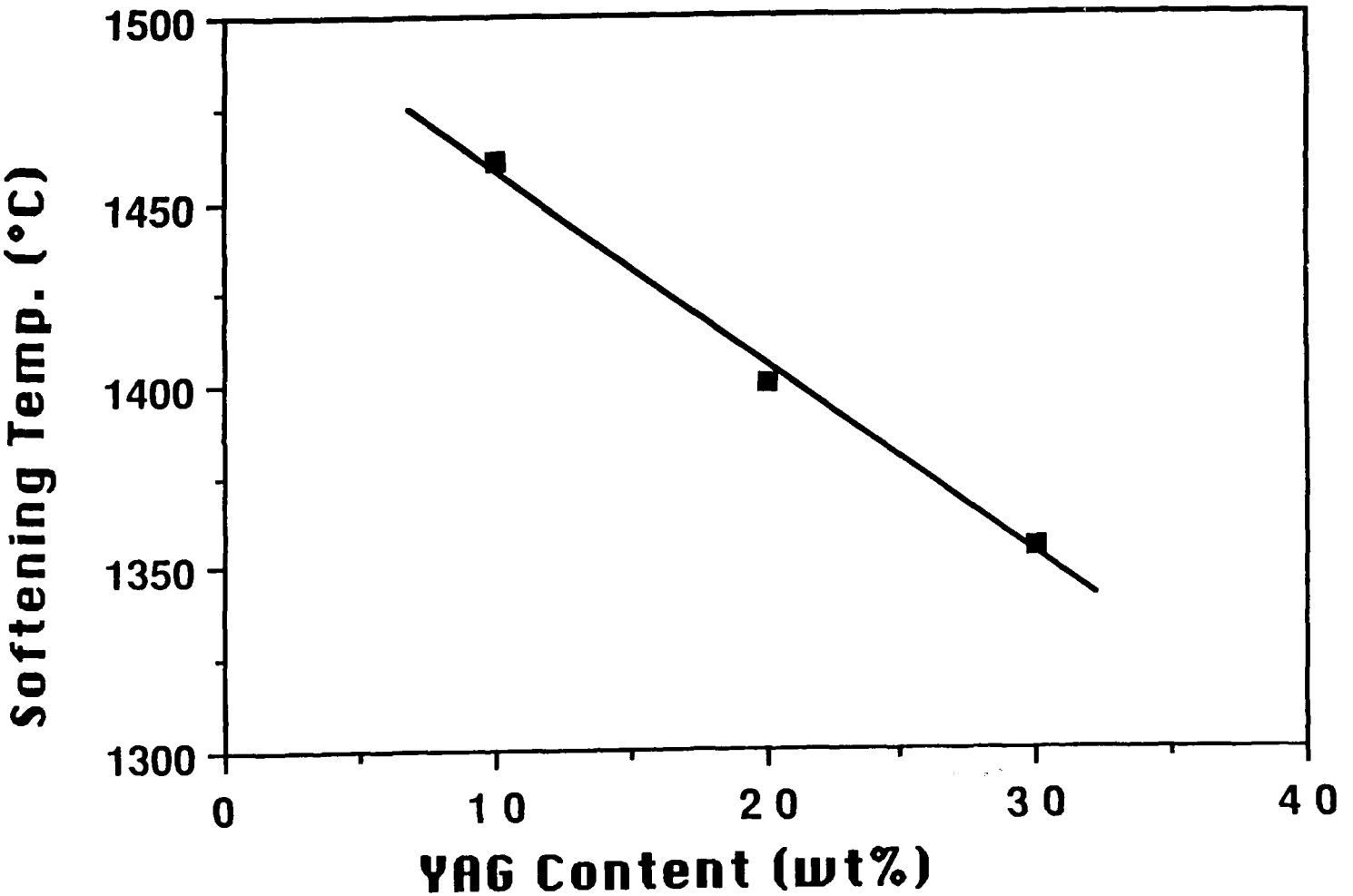

Fig. 5 Softening temperature vs YAG content

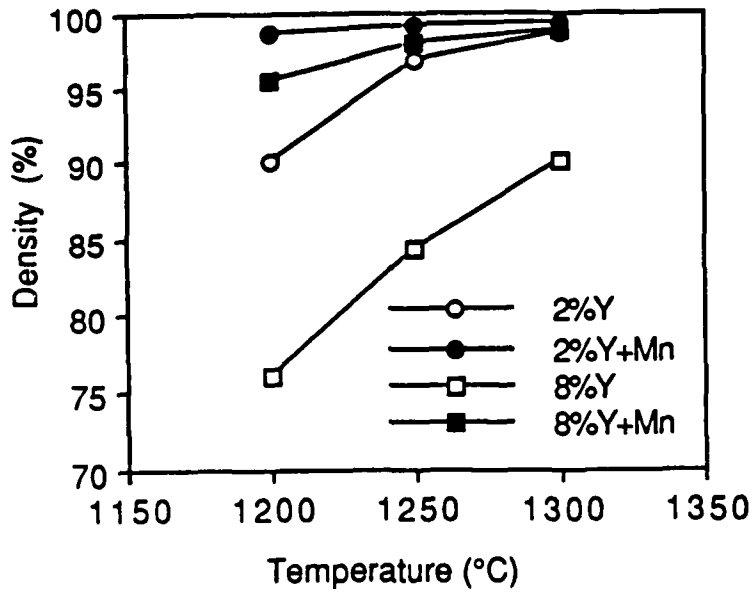

Fig. 6 Sintered density of tetragonal (2Y) and cubic (8Y) zirconia vs sintering temperature

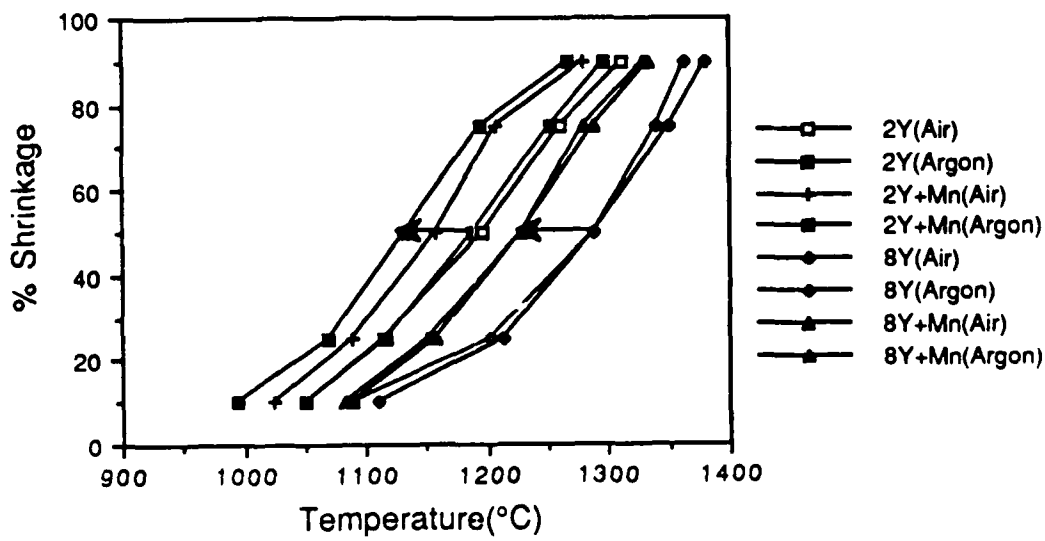

Fig. 7 Isochronal heating dilatometry curves of various tetragonal (2Y) and cubic (8Y) zirconia

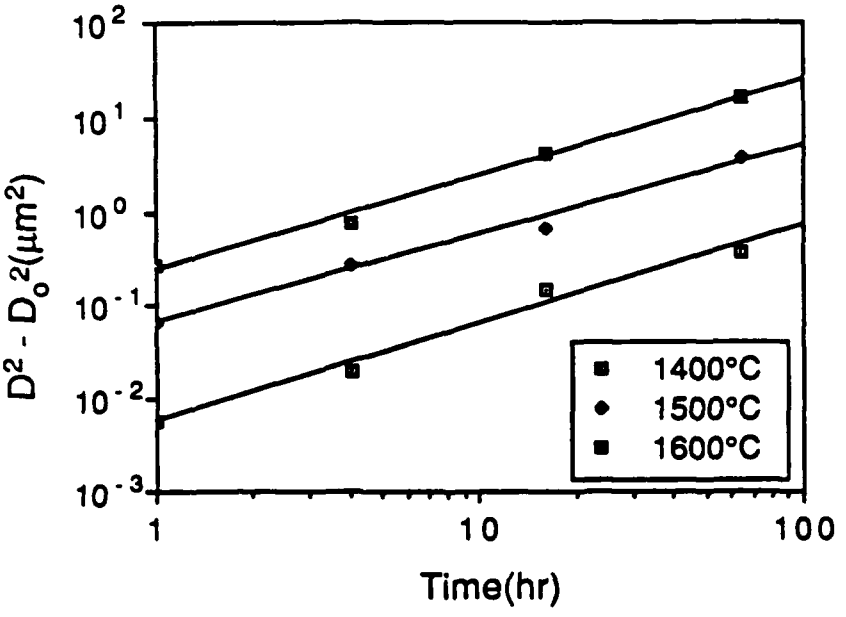

Fig. 8 Grain growth of Mn doped 2 mol% Y_2O_3-ZrO_2

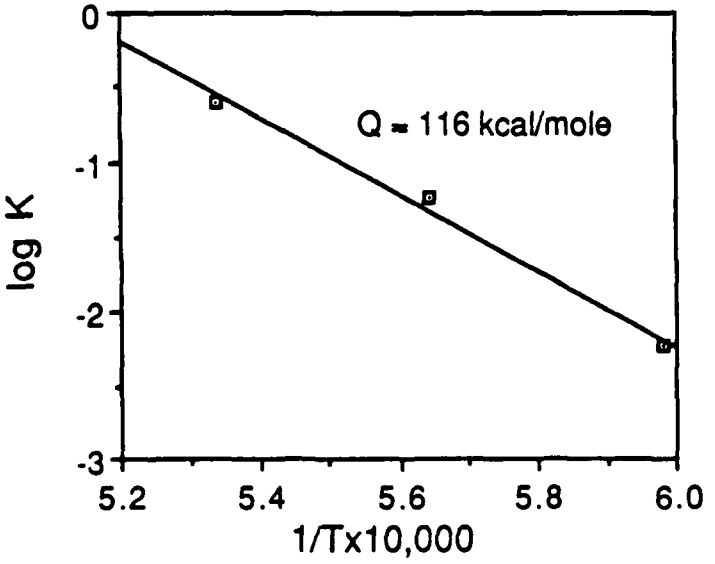

Fig. 9 Activation energy of Mn doped 2 mol % Y_2O_3-ZrO_2

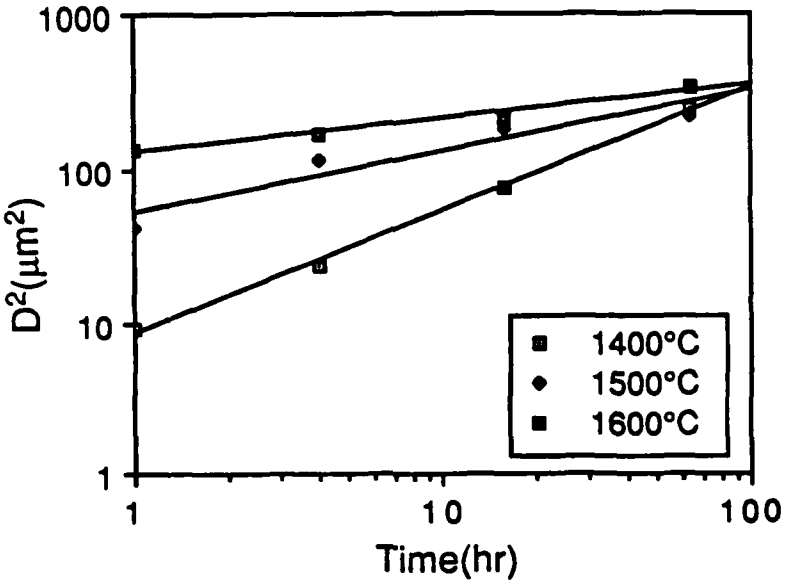

Fig. 10 Grain growth of Mn doped 8 mol% Y_2O_3-ZrO_2

APPENDIX 1

ANISOTROPIC GRAIN GROWTH DURING FINAL STAGE SINTERING OF SILICON NITRIDE CERAMICS

C.M. Hwang, T.Y. Tien, and I-Wei Chen
Department of Materials Science and Engineering
The University of Michigan
Ann Arbor, Michigan 48109-2136
U.S.A.

ABSTRACT

The kinetics of grain growth of ß SiAlON are reported for a broad range of compositions containing YAG and cordierite additives. Anisotropic growth favoring a prismatic morphology was found in all cases. Both the length and the width of the grains follow a cubic growth law. The activation energies were determined to be between 145 and 180 Kcal/mole. High resolution TEM examination revealed a rounded growth front along the [001] direction and a sharp interface with very few ledges along the [210] direction. A growth model, which envisions continuous growth in the [001] direction and lateral ledge growth in the [210] direction, appears to provide a satisfactory explanation of these observations.

INTRODUCTION

Grain growth during the final stage of liquid phase sintering is commonly reported to follow a cubic law analogous to Ostwald ripening. Both diffusion through the liquid and interface reactions at the solid/liquid interface are possible rate-controlling mechanisms [1]. Most theoretical analyses and model experiments have been conducted for isotropic systems consisting of equiaxed grains. In silicon nitride ceramics, however, grain shapes are very anisotropic, with β-SiAlON grains growing as hexagonal prisms along the [001] direction [2]. An example of such microstructure is shown in Fig. 1. Anisotropic grain growth in liquid phase sintering of this system has not been quantitatively studied. This investigation reports on the kinetics of grain growth and on the structure of solid/liquid interfaces in ß-SiAlON with $Y_3Al_5O_{12}$ (YAG) and $Mg_2Al_4Si_5O_{18}$ (cordierite) additions. Based on these experimental observations, a model is proposed to account for the anisotropic growth behavior.

EXPERIMENTAL

SiAlON solid solutions were prepared in the system Si, Al, X/O, N, with X = Y or Mg. The ß solid solution compositions are shown in Fig. 2. The compositions were sintered in a nitrogen atomsphere between 1400° and 1800°C. The kinetics of both densification during sintering and the accompanying α to ß phase transformation were already reported in the companion paper [3]. Data for grain growth were taken after the completion of the phase transformation. High resolution electron microscopy was performed using a JOEL 2000FX microscope operating at 200KV.

RESULTS

The growth rates of ß grains in the SiAlON-YAG system are shown in Fig. 3 for the [001] direction (length) and the [210] direction (width). The rates are highly anisotropic and can be expressed in the form:

$$d^n - d_o^n = K(t-t_o) \quad (1)$$

where d is the average grain dimension at time t, d_o is the dimension at time t_o. A cubic law, n=3, was found to be consistent with all of the growth data, in both directions and in both systems. The rate constant, K, is relatively insensitive to the amount of the liquid (Fig. 4), but very sensitive to the alumina content as shown in Fig. 5. A higher growth rate was found in the SiAlON-YAG system (Fig. 6). The activation energy of the rate constant was found to be about 160 Kcal/mole for the SiAlON-YAG system and about 170 Kcal/mole for the SiAlON-cordierite system. Similar to the difference in the kinetics of densification and phase transformation discussed in the companion paper [3], grain growth in the SiAlON-cordierite system is consistently slower than that in the SiAlON-YAG system. This is due to the difference in liquid viscosity in the two systems which results from the difference in the silica content of the liquids.

Further insight into the growth anisotropy was provided by examination of the solid/liquid interface using high resolution electron microscopy. A micrograph of a lattice image of a ß grain in the SiAlON-YAG system is shown in Fig. 7a. The structure of this grain, which is mostly enclosed in a glassy phase, was identified by diffraction analysis as shown in the figure. The semi-spherical cone in the [001] growth front is clearly shown in Fig. 7b, which indicates the presence of continuous growth steps characteristic of a diffuse interface. Along the [210] growth front, the interface is sharp except for a ledge as shown in Fig. 7c. These structures are suggestive of different growth kinetics which are in turn responsible for the anisotropic grain shape.

MODEL OF ANISOTROPIC GRAIN GROWTH

The model we propose here assumes continuous growth on the diffuse interface in the [001] direction and lateral growth by a ledge mechanism on the sharp prismatic planes in the [210] directions. The model is schematically depicted in Fig. 8. We represent the volume of the prism by

$$v = \pi l r^2 \quad (2)$$

where l is the length and r is the root mean square radius of the cross section. The growth rate is given by

$$dv/dt = \pi r^2\, dl/dt + 2\pi l r\, dr/dt \quad (3)$$

In the above, the first term is the growth rate in the [001] direction and the second term is the growth rate in the [210] directions. The normalized driving force for grain growth is taken to be

$$F = \gamma\Omega/kTr \quad (4)$$

where γ is the normalized solid/liquid energy of the prismatic planes, Ω is the molecular volume, and kT has its usual meaning.

The growth rates in the two directions are respectively given by

$$dl/dt = DcF/r \quad (5)$$

and

$$dr/dt = DcF/l \quad (6)$$

In the above, D is the solute diffusivity in the liquid which is used to relate the jump probability at the solid/liquid interface, and c is the solute concentration in the liquid. Here,

we have assumed diffusion control in both cases and a perfect sink efficiency at the diffuse (00•1) interface and along the ledge on the (10•0) prismatic planes. Only lattice sites facing the [001] direction are counted. Additional geometric considerations, which will slightly affect the growth rates at low volume fractions of liquid, have been omitted in both expressions.

Because of the diffusion dependence of the growth equations given above, it is clear that the origin of the growth anisotropy for these grains lies in the disparity of available growth sites for the two types of solid/liquid interfaces. Following a simple manipulation of Eqs. 4-6, we confirm that a cubic law is followed by both l and r. As expected, their rate constants are both proportional to $Dc\gamma\Omega/kT$, but otherwise differ by a factor of $(l_0/r_0)^3$, strongly favoring growth in the length direction. Here, l_0 and r_0 are the grain length and radius, respectively, at time t_0.

DISCUSSIONS

Phenomenologically, anisotropic grain growth in the present systems seems to be consistent with the diffusion control mechanism outlined above. The key observations in support of this argument are (a) growth exponents being 3; (b) kinetics sensitive to liquid viscosity but not to liquid fractions; and (c) similar activation energies in both the sharp [210] and diffuse [001] growth directions. Note that (b) is not consistent with interface reaction control; furthermore, in contrast to (c), a higher activation energy for the sharp interface is expected for interface reactions.

The presence of a ledge on (10•0) prismatic planes can be thought of as due to a screw dislocation in the [001] direction. As a common origin providing growth steps on an atomically sharp interface, a screw dislocation normal to such a plane generates a spiral growth step which expands outward at a constant radial velocity [4]. Simple calculations pertinent to Ostwald ripening of prismatic grains have verified, however, that the critical radius of the spiral in the present case is of the order of r. Hence, only one spiral turn can fall on the six prismatic (10•0) surfaces. Indeed, in Figure 7c, only one growth step can be seen on the side surface. As this growth step sweeps over (10•0) surfaces by one turn, the prism grows in the width direction by one molecular layer.

ACKNOWLEDGEMENT

This research was supported by US Department of Energy, Office of Basic Energy Sciences, Materials Science Division, under Grant No. DE-FG02084-ER45069. One of us (I-W. C) also acknowledges the support by US Air Force, under Grant No. AFOSR-87-0289. The experimental assistance of H. Hohnke is gratefully appreciated.

REFERENCES

1. R.M. German, Liquid Phase Sintering, Plenum Press, New York (1985).
2. H. Hohnke and T.Y. Tien, Progress in Nitrogen Ceramics, Martinus Nijhoff, Netherlands (1983).
3. C.M. Hwang and T.Y. Tien, the companion paper (1987).
4. F.C. Frank, *Discussions Faraday Soc.*, 5, 46 (1949).

Fig. 1 A typical SEM microstructure of ß-SiAlON ceramics. (bar = 5 μm)

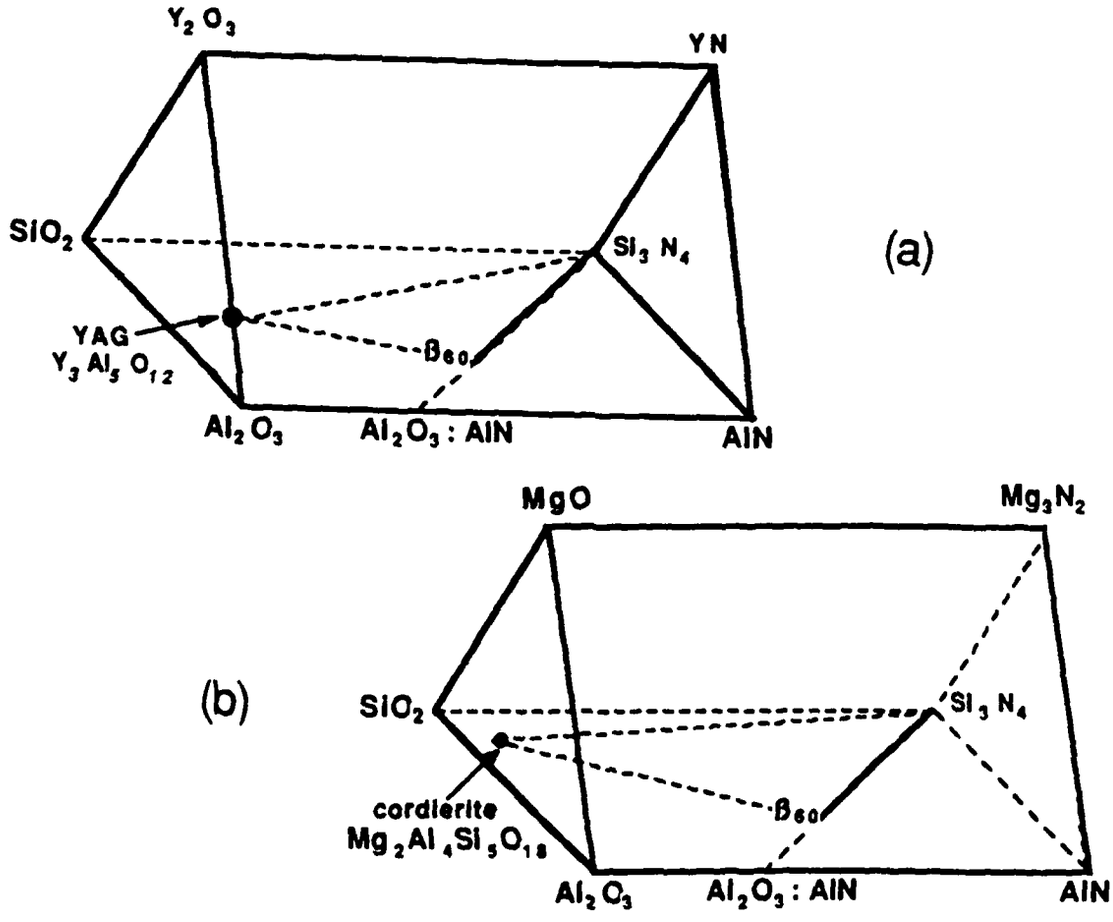

Fig. 2 The phase diagrams in the system Si, Al, X/O, N, with (a) X=Y and (b) X=Mg.

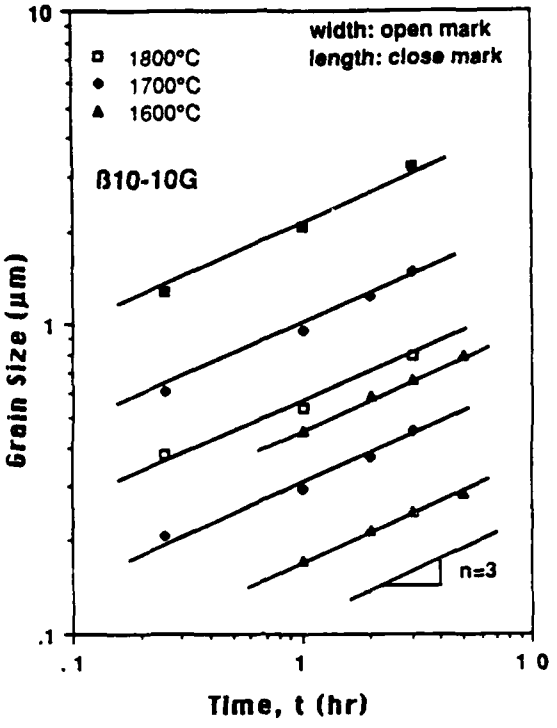

Fig. 3 Grain growth as a function of sintering temperature in the system SiAlON-YAG.

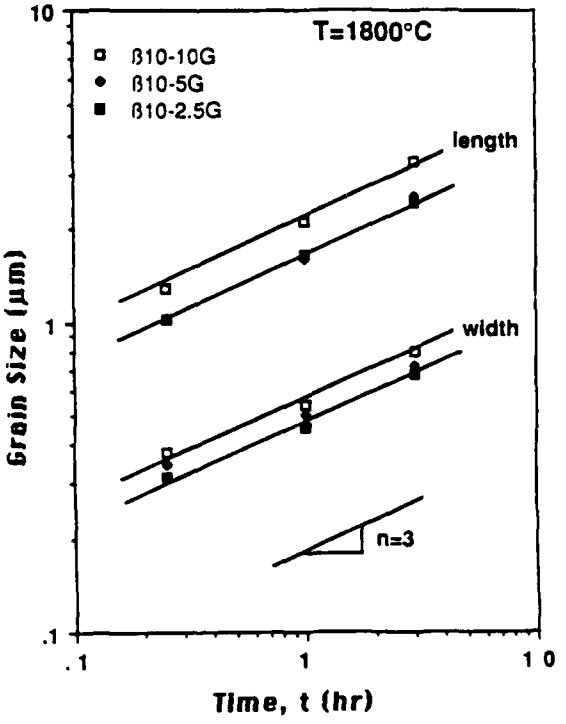

Fig. 4 Grain growth as a function of additive content in the system SiAlON-YAG.

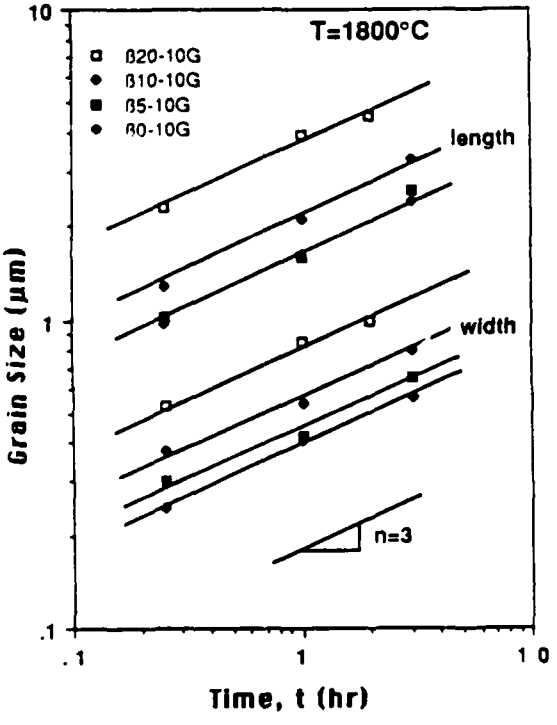

Fig. 5 Grain growth as a function of Al eq.% in the SiAlON composition in the system SiAlON-YAG.

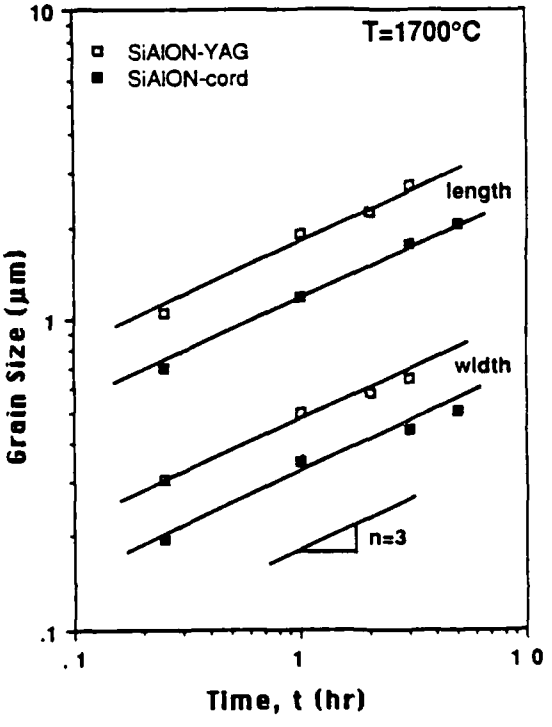

Fig. 6 Comparison of grain growth kinetics in the systems SiAlON-YAG and SiAlON-cordierite.

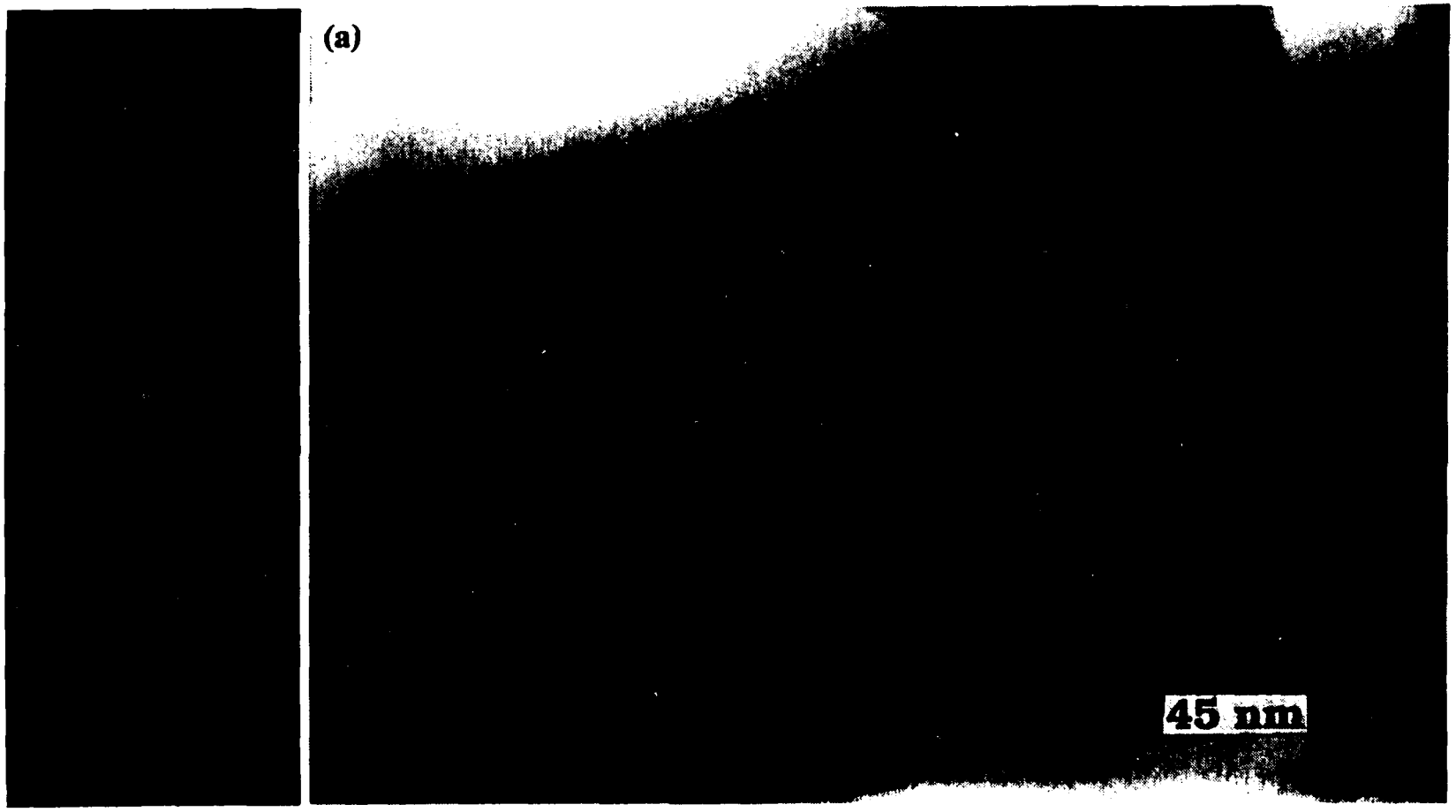

Figure 7. (a) A typical ß grain in SiAlON ceramics. The grain elongates in the [001] direction. (b) The enlarged view of the "rough" growth front in the [001][direction. (c) The enlarged view of the "smooth" growth front in the [210] direction. One growth ledge is spoted (arrowed).

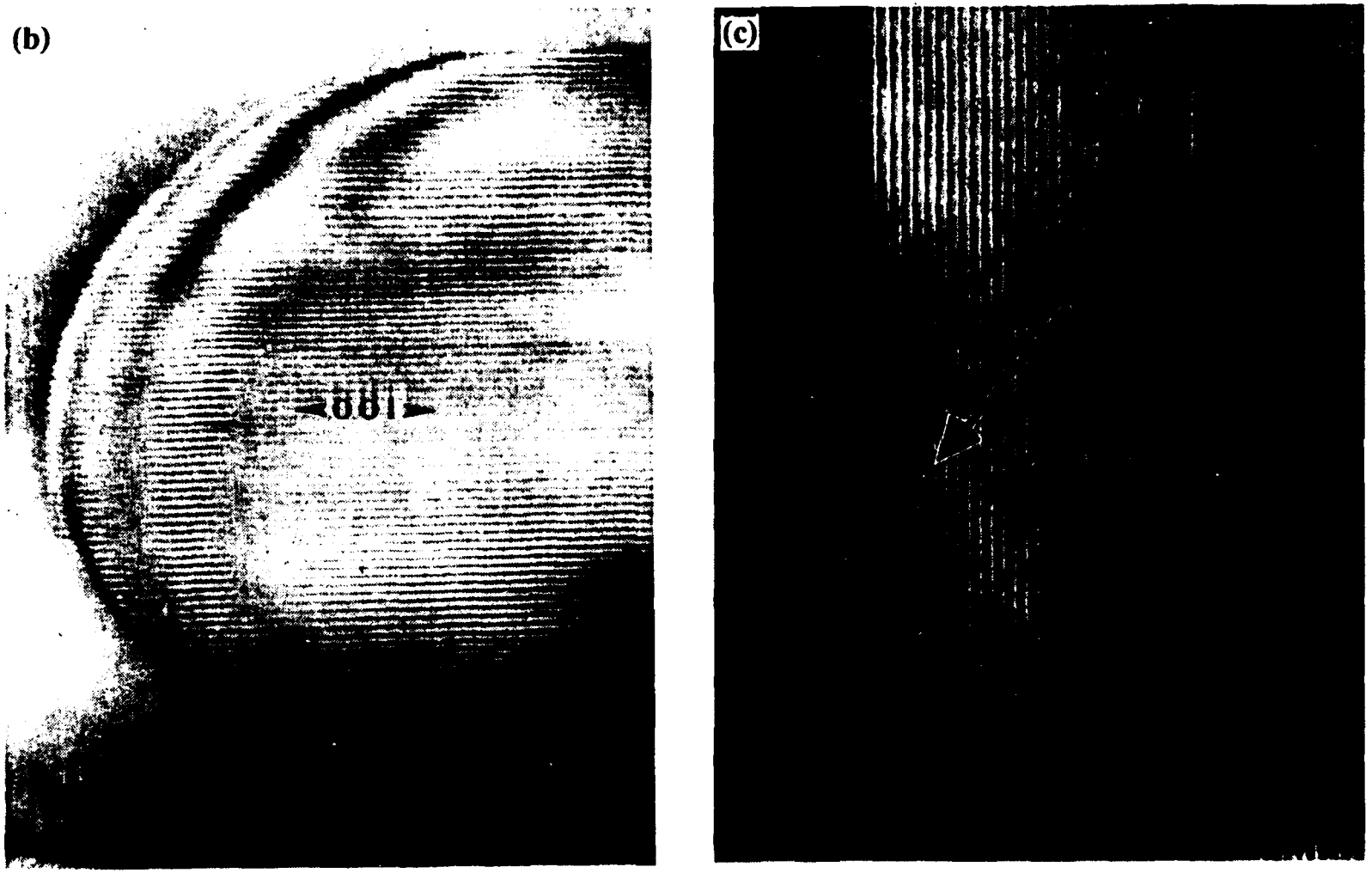

Figure 7. ----- continued.

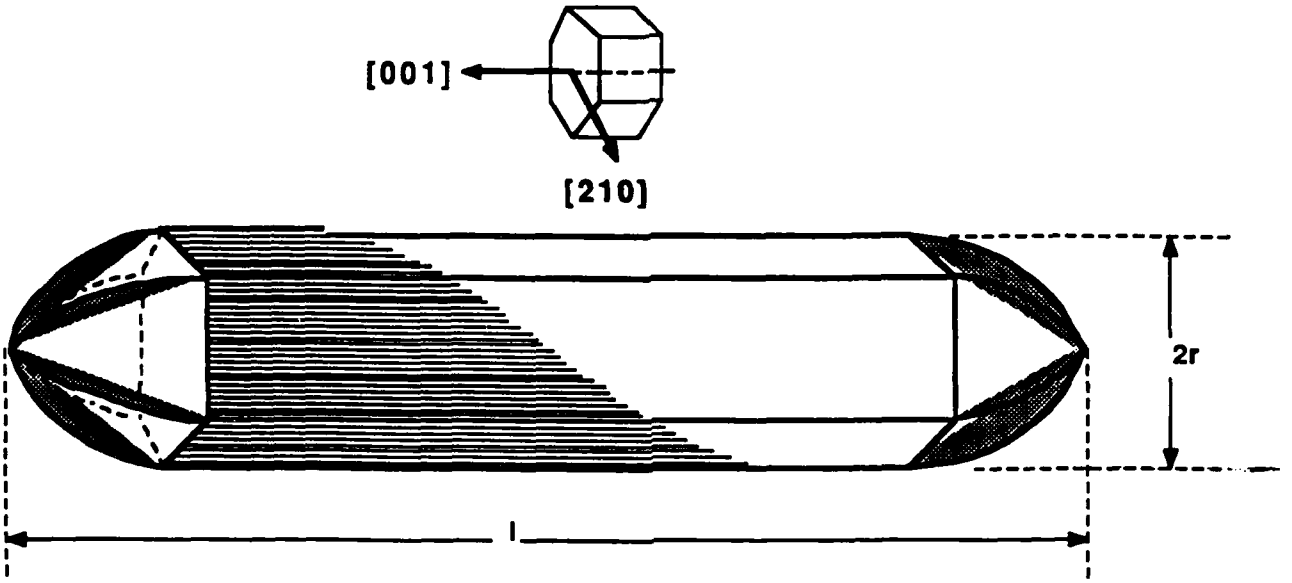

Fig. 8 Schematics of a ß Grain in the process of anisotropic growth

APPENDIX 2

SINTERING AND GRAIN GROWTH IN TETRAGONAL AND CUBIC ZIRCONIA

I.G. Lee and I-Wei Chen
Department of Materials Science and Engineering
The University of Michigan
Ann Arbor, Michigan 48109-2136

ABSTRACT

The different sinterability of tetragonal and cubic zirconia can be attributed to their different behavior of grain growth. Growth rate of cubic grains in 8 m/o Y_2O_3-ZrO_2 was found to be 30 to 250 times faster than that of tetragonal grains in 2 m/o Y_2O_3-ZrO_2. Although grain growth in both materials follows the parabolic law, the activation energy is 105 Kcal/mole for the tetragonal zirconia and 69 kcal/mole for the cubic zirconia. Measurements of dihedral angles revealed a larger grain boundary energy in the cubic phase than in the tetragonal phase. The possible origins of their different behavior are discussed.

INTRODUCTION

In order to achieve full densification, excessive grain growth has to be suppressed in firing. Experience with zirconia systems has provided ample evidence that the grain size of the cubic phase is much larger than that of the tetragonal phase, suggesting the possibility of a lower sintered density in the cubic phase regime. Indeed, this is confirmed in many zirconia systems. As an example, Fig. 1 shows the compositional dependence of sintered densities of ZrO_2-Y_2O_3 and ZrO_2-In_2O_3 ceramics. The decreased densities in the cubic phase are quite evident for both. Examinations of the sintered microstructures revealed large cubic grains containing intragranular pores in the cubic phase regime. Thus the role of grain growth in sintering of zirconia ceramics appears to be a classical one: a faster grain growth causes pore detachment from grain boundaries, preventing full densification. To afford a better control of sintering of these ceramics, it is clearly necessary to understand the mechanistic origin of the large disparity of grain growth in the two zirconia phases. The purpose of this paper is to report on the grain growth kinetics and grain boundary characteristics for both tetragonal and cubic zirconia, and to provide a rationale for their different behavior.

EXPERIMENTAL

Coprecipitated zirconia powders containing 2 to 8 m/o Y_2O_3 were used in this study. Pellets were sintered between 1300°C and 1700°C in air for various time. Grain sizes were measured by the linear intercept method, with the reported values being 1.56 times

the average intercept lengths. Grain growth in initial and intermediate stage sintering was investigated at 1400°C for shorter time, using rapidly heated specimens. Dihedral angles between tetragonal and cubic phases were measured using specimens containing both phases (at 4 m/o and 6 m/o Y_2O_3).

RESULTS

Data of grain size of 2 and 8 m/o Y_2O_3 as a function of sintering are shown in Figs. 2 and 3. Between 1300°C and 1700°C, the 2 m/o Y_2O_3 samples are entirely tetragonal; while at 8 m/o Y_2O_3, they are entirely cubic. Both sets of data obey the parabolic growth law,

$$d^2 - d_o^2 = K\,(t-t_o) \qquad (1)$$

where d is the grain size at time t, d_o is the grain size at time t_o, and K is a rate constant. The rate constant for the cubic phase is 30 times to 250 times larger than that for the tetragonal phase, reflecting a ratio of grain sizes of 5 to 10. The activation energies of the rate constants are 105 Kcal/mole for the tetragonal grain growth and 69 Kcal/mole for the cubic grain growth, as shown in Fig. 4.

Grain growth in the two phase regimes are difficult to assess quantitatively, due to the lack of compositional contrast between the two phases in scanning electron microscopy and the poor statistics for grain size measurements in transmission electron microscopy. Nevertheless, qualitatively, we were able to identify the cubic grains which always grow to larger sizes than those of the tetragonal grains. This is the case both for 4 m/o Y_2O_3, when the cubic grains are mostly surrounded by the tetragonal grains, and for 6 m/o Y_2O_3, when the cubic grains form a continuous majority matrix. Dihedral angles at triple points of two cubic grains and one tetragonal grain are related to the cubic grain boundary energy γ_{cc} and the c/t phase boundary energy γ_{tc}. This can be seen in Fig. 5a. Likewise, dihedral angles at triple points of two tetragonal grains and one cubic grain are related to the tetragonal grain boundary energy γ_{tt} and γ_{tc}, as shown in Fig. 5b. The dihedral angle θ_{cc} in Fig. 5a is smaller by about 30° than the dihedral angle θ_{tt} in Fig. 5b. Using the following relationship

$$2\gamma_{tc}\cos(\theta_{tt}/2) = \gamma_{tt} \qquad (2)$$

$$2\gamma_{tc}\cos(\theta_{cc}/2) = \gamma_{cc} \qquad (3)$$

with the dihedral angles listed in Table 1, the ratios of interfacial energies were determined.

Table 1. Measured dihedral angles

	4 m/o Y_2O_3	6 m/o Y_2O_3
θ_{tt}	134±7°	131±7°
θ_{cc}	97±11°	105±10°

Their average can be represented as the following ratios

$$\gamma_{cc} : \gamma_{tc} : \gamma_{tt} = 1 : 0.76 : 0.63 \qquad (4)$$

Grain growth in the initial and intermediate stages was also investigated. These data will be published elsewhere. At 1400°C, it was found that the densification rates of 2 m/o and 8 m/o samples are essentially the same during the initial and intermediate stage of

sintering. The activation energies were not determined, since they will be affected by the activation energy of densification. The latter has been reported to be around 96 Kcal/mole for CaO stabilized cubic zirconia (13 m/o CaO).[1]

DISCUSSIONS

Our results on both tetragonal and cubic zirconia demonstrate that both undergo normal grain growth in the temperature range studied. The activation energy of the tetragonal phase is higher than the cubic phase. Although there has been no systematic report on grain growth of tetragonal zirconia in the literature to the authors' knowledge, our findings on cubic zirconia are consistent with a previous study of CaO stabilized cubic zirconia (16 m/o CaO) which gave a growth exponent of 0.4 and an activation energy of 80 Kcal/mole.[2]

Two considerations of normal grain growth are (a) driving force and (b) mobility of grain boundaries. The dihedral angle measurements have established that the driving force for grain growth is the largest for cubic zirconia, intermediate for cubic or tetragonal grains in a mixed-phase matrix, and smallest for an entirely tetragonal zirconia. Although this aspect is consistent with the contrasting grain sizes of the two phases in all three types of microstructures, it can not be the sole reason for the much faster growth rate in the cubic phase. Our data indicate that a difference of up to 250 times is seen in the rate constant K, yet grain boundary energies differ by less than a factor of 2. Further explanation must be sought elsewhere to explain the grain growth behavior.

It appears that the mobility of the cubic grains is much higher than that of the tetragonal grains. One possibility is that the boundary diffusivity of the cubic grains is higher. This can be explained by referring to the theory of Borisov *et al.*[3]which couples the thermodynamic consideration to grain boundary diffusion,

$$\gamma_b = A\,RT\,\ln(D_b/D_l) \qquad (5)$$

In the above, γ_b is the boundary energy, D_b is the boundary diffusivity, D_l is the lattice diffusivity, A is a geometric constant related to the atomic area on the grain boundary and to the jump statistics, and RT has its usual meaning. This model has been verified in many metallic alloys[4] and at least in one ceramic system (i.e. yttria-doped alumina)[5]. Hence a lower boundary energy is predicted to be accompanied by a lower boundary diffusivity and a higher activation energy. This prediction is consitent with our data, if we assume a proportionality between K and boundary diffusivity.

The large difference in grain boundary energies and diffusivities in the two phases could be due to a different behavior of solute segregation in the two materials. For example, an enrichment of yttrium on the tetragonal boundary but not on the cubic boundary can generate such an effect. Indeed, for certain solutes which segregate over a longer spatial extent, it is expected that boundary mobility may be controlled by solute drag, which involves lattice diffusion. The activation energy for grain growth in tetragonal zirconia is 105 Kcal/mole, which is comparable to that of self diffusion of yttrium cations in a yttria stabilized cubic lattice (102Kcal).[6] The activation energy of boundary diffusivity in yttria stabilized cubic zirconia is 70 Kcal/mole,[6] which is closer to the activation energy for grain growth in cubic zirconia. It should also be noted that the presence of a grain boundary glassy phase in tetragonal zirconia could decrease the apparent grain boundary energy and increase the diffusion distance across the boundary.

It is recalled that both ionic conductivity[7-8] and densification rate in hot pressing[9] exhibit a strong yttria compositional dependence in the present system. That is, both cation and anion (lattice) diffusivities increase when the yttria content increases from 5 to 8 m/o. Although this phenomenon of enhanced kinetics is pronounced and probably general in all lightly doped zirconia [10] its magnitude is still a factor of 3 to 10 smaller than the enhancement of the rate constants K in grain growth in the same compositional range. Nevertheless, together with the consideration of grain boundary energies, it could present an alternative rationale for the observed different growth behavior.

Concerning sintering schedule, Wu and Brook[11] suggested that fast firing to higher

temperature is preferrable for sintering zirconia. Their suggestion was based on the observation that the activation energy of densification [1] is higher than that for grain growth[2] in CaO stabilized cubic zirconia.[2] While this recommendation is sound for cubic zirconia, it is not likely to be useful for tetragonal zirconia in view of the much higher activation energy of grain growth reported in this study. Indeed, our experience found that slow firing at low temperatures yielded the best results for tetragonal zirconia in most cases.

ACKNOWLEDGEMENTS

This research is supported by the US Air Force Office of Scientific Research, under Grant No. AFOSR-87-0289. We are grateful to Dr. Jie Xu for providing unpublished data on In_2O_3 stabilized ZrO_2.

REFERENCES

1. P.J. Jorgensen, in *Sintering and Related Phenomena*, p. 401, eds. G.C. Kuczynski, N.A. Hooton and C.F. Gibbon, Gordon and Breach, New York (1967).
2. T.Y. Tien and E.C. Subbarao, *J. Am. Ceram. Soc.*, **46**, 10, 489-492 (1963).
3. V.T. Borisov, V.M. Golikov, and G.V. Scherbedinskiy, *Phys. Metals Metallograph*, **17**, 80 (1964).
4. D. Gupta, *Metall. Trans.* **8A**, 1431 (1977).
5. P.Nanni, C.T.H. Stoddart, and E.D. Hondros, *Mater. Chem.*, **1**, 297 (1976).
6. Y.Oishi, K. Ando, and Y. Sakka, Advances in Ceramics, Vol.7, 208-219 (1983).
7. T.M. Dixon, L.D. LaGrange, U. Merten, C.F. Miller and J.T. Porter II, *J. Electrochem. Soc.* **110**, 276 (1963).
8. D.W. Strickler and W.G. Carlson, *J. Amer. Ceram. Soc.* **47**, 122 (1964).
9. S. Wu and R.J. Brook, *Solid State Ionics*, *14*. 123 (1984).
10. T.Y, Tien and E.C. Subbarao, J. Chem, Phys. **39**, 1041 (1963).
11. S. Wu and R.J. Brook, *Advances in Ceramics*, **12**, 693 (1984).

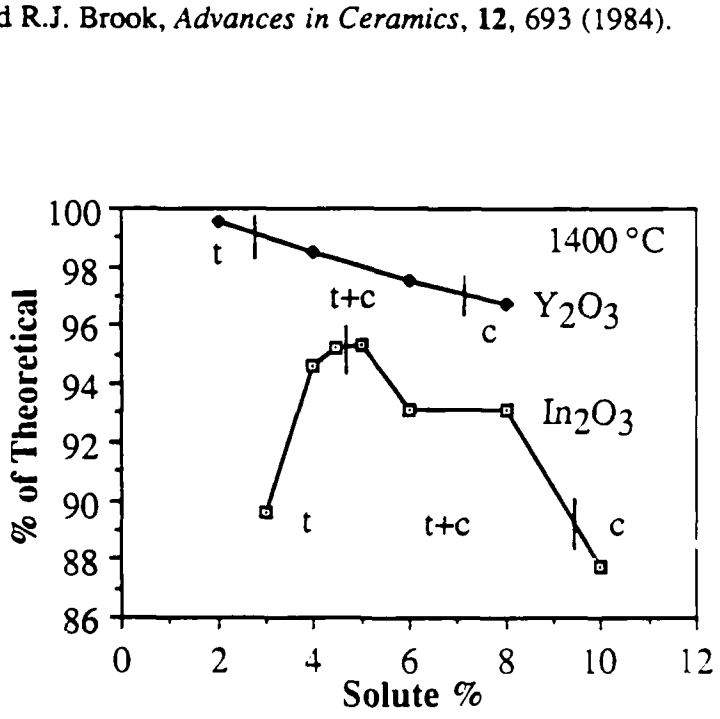

Fig. 1. Sintered density at 1400°C as a function of stabilizer content

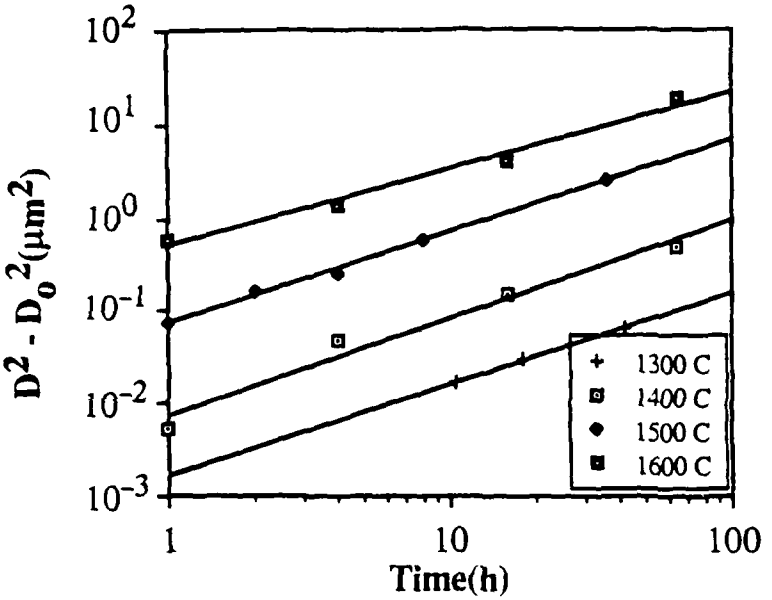

Fig. 2. Grain growth kinetic for 2 m/o Y_2O_3-ZrO_2(tetragonal)

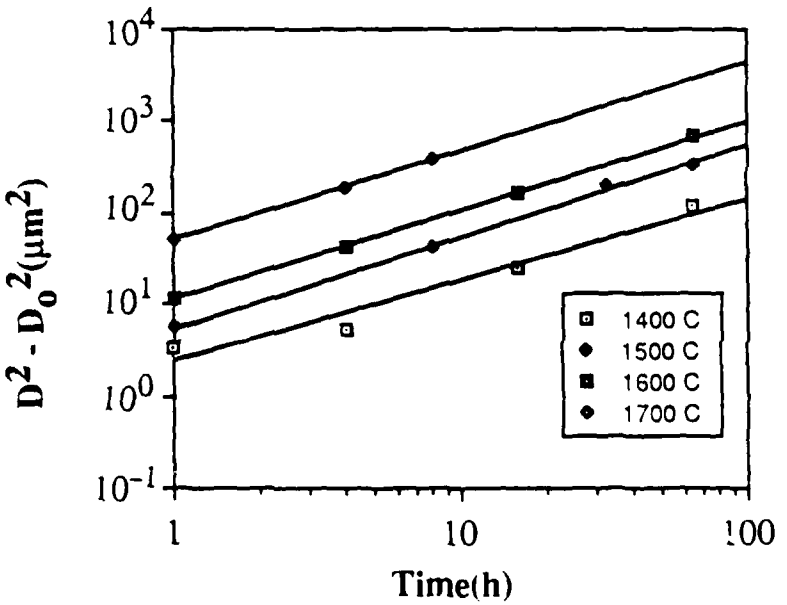

Fig. 3. Grain growth kinetics for 8 m/o Y_2O_3-ZrO_2(cubic)

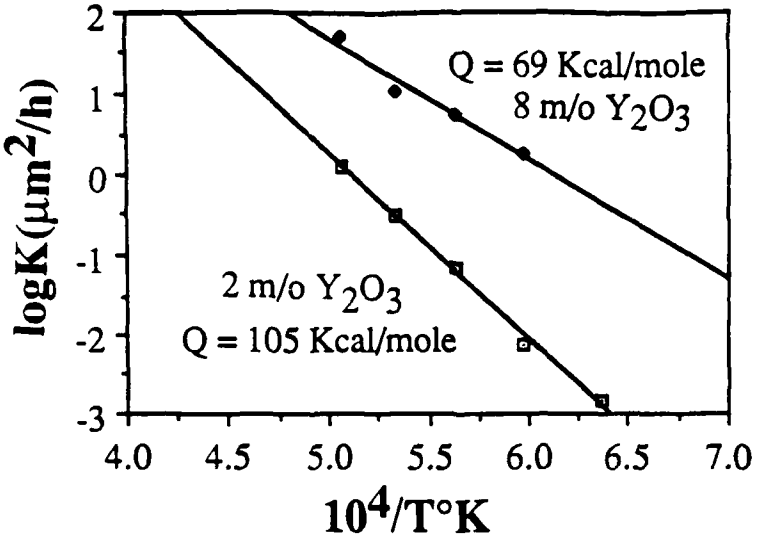

Fig. 4. Activation energies of grain growth in cubic and tetragonal zirconia

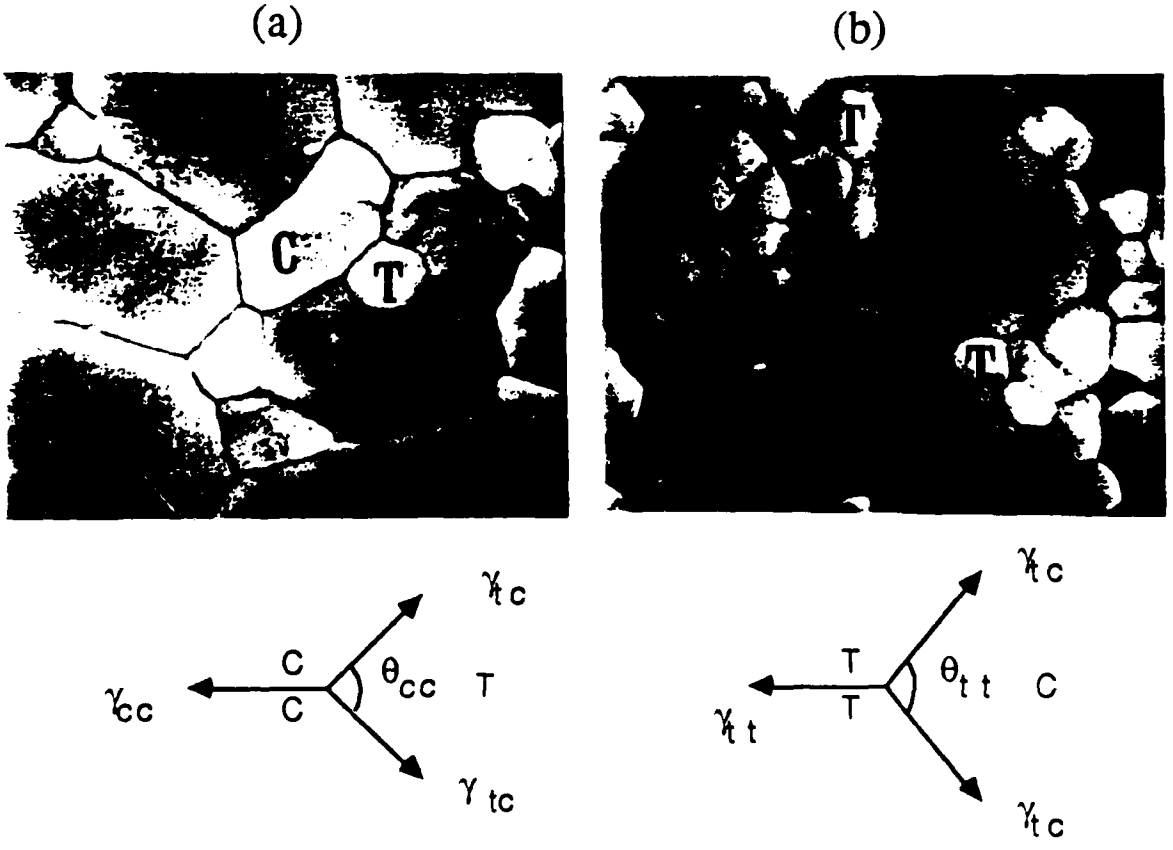

Fig. 5. Relationship between dihedral angles and interfacial energies
(a) a tetragonal grain surrounded by cubic grains in 6 m/o Y_2O_3-ZrO_2
(b) cubic grains surrounded by tetragonal grains in 4 m/o Y_2O_3-ZrO_2